

# Renormalization footprints in the phase diagram of the Grosse-Wulkenhaar model

Dragan Prekrat\*

University of Belgrade, Faculty of Physics, P.O. Box 44, SR-11001 Belgrade, Serbia

(Dated: November 26, 2023)

We construct and analyze a phase diagram of a self-interacting matrix field coupled to curvature of the non-commutative truncated Heisenberg space. In the infinite size limit, the model reduces to the renormalizable Grosse-Wulkenhaar's. The curvature term is crucial to renormalization. When turned off, the triple point collapses into the origin as matrices grow larger. When turned on, the triple point shifts away proportionally to the coupling strength and matrix size. Coupling attenuation that renormalizes the Grosse-Wulkenhaar model cannot subdue the shifting, and the translational symmetry-breaking stripe phase escapes to infinity, taking away the problematic UV/IR mixing.

## I. INTRODUCTION

We are often challenged to explain what we do in just a few words. What springs to mind in connection to non-commutative QFT is: CERN in Wonderland. A realm where space and time behave oddly and the rules are a bit off. As if that were not enough, even the chit-chat<sup>1</sup> at the Hatter's tea party seems to be inspired by the non-commutative quaternions [2].

Some seven decades later, non-commutativity (NC) arrived from Wonderland to Quantumland, settling first in the canonical relation between position and momentum and shortly after into NC space-time. It was first invoked in the hope of resolving the confusion about the infinities in the nascent quantum field theory [3], but the trick of renormalization beat it to the punch. Since then, it occasionally reemerged, both in fundamental and effective form, from condensed matter physics to quantum gravity [4, 5]. Finally, when NC was discovered in the low energy sector of the string theory at the turn of the millennium [6], various new NC models followed.

The parallel with Wonderland continues in an uncanny manner. Just as the bites from opposing sides of the magic mushroom threaten to shrink or stretch Alice in a runaway fashion, divergencies of non-planar Feynman diagrams spill from high energy to low energy sector, spoiling the renormalizability of NC QFTs [7–10]. And just like the problem with the mushroom, UV/IR mixing can be resolved only by proper balancing of large and small scales, in the guise of the Langman-Szabo duality [11].

Grosse-Wulkenhaar (GW) model [12–14]

$$S_{\text{GW}} = \int \frac{1}{2}(\partial\phi)^2 + \frac{\Omega^2}{2}((\theta^{-1}x)\phi)^2 + \frac{m^2}{2}\phi^2 + \frac{\lambda}{4!}\phi^4 \quad (1)$$

managed to evade the UV/IR mixing. It features a self-interacting real scalar field on the Moyal space equipped with a  $\star$ -product

$$f \star g = f e^{i/2 \bar{\partial}\theta\bar{\partial}} g \Rightarrow [x^\mu, x^\nu]_\star = i\theta^{\mu\nu}. \quad (2)$$

Its potential is enhanced by the external harmonic oscillator term of a possible gravitational origin. Namely, the model can be reinterpreted [15] as that of a scalar field in a curved NC space

$$S_R = \int \sqrt{g} \left( \frac{1}{2}(\partial\phi)^2 - \frac{\xi}{2}R\phi^2 + \frac{M^2}{2}\phi^2 + \frac{\Lambda}{4!}\phi^4 \right). \quad (3)$$

The oscillator term, which holds a key to renormalizability, is now seen as a coupling to the curvature of the underlining truncated Heisenberg algebra  $\mathfrak{h}^{\text{tr}}$

$$[\mu x, \mu y] = i\epsilon(1 - \mu z), \quad (4a)$$

$$[x, z] = +i\epsilon\{y, z\}, \quad [y, z] = -i\epsilon\{x, z\}, \quad (4b)$$

projected onto  $z = 0$  section. Another possible source of the oscillator term was presented in [16], where it elegantly appears in the expansion of the kinetic term of the free scalar field that is situated in the Snyder-de Sitter space. This model also predicts the running of the curvature coupling, which is an essential ingredient of the GW-renormalizability. It would be interesting to see if similar conclusions could be reached in fuzzy de Sitter space as well [17, 18].

UV/IR mixing still poses a problem for gauge fields on NC spaces [19]. Hoping to build on the GW model's success, [20, 21] tried to adapt it to a gauge field on  $\mathfrak{h}^{\text{tr}}$ . Still, after extensive treatment, we found non-renormalizability lurking in the form of divergent non-local derivative counterterms [22]. Apart from the trivial vacuum, this model contains another, which breaks the translational invariance:

$$A_1 = -\frac{\mu^2 y}{\epsilon g}, \quad A_2 = +\frac{\mu^2 x}{\epsilon g}, \quad \phi = \frac{\mu}{\epsilon g}. \quad (5)$$

This echoes the translational symmetry-breaking stripe phase that seems to be at the root of UV/IR mixing.

\* dprekrat@ipb.ac.rs

<sup>1</sup> "Then you should say what you mean," the March Hare went on.

"I do," Alice hastily replied; "at least—at least I mean what I say—that's the same thing, you know."

"Not the same thing a bit!" said the Hatter. "You might just as well say that 'I see what I eat' is the same thing as 'I eat what I see'!" [1]

“Stripes” refer to patterns of spatially non-uniform magnetization, which appear when the field oscillates around different values at different points in space [23–25]. They also seem to shatter the symmetry between large and small scales that keeps the UV/IR mixing at check: locally, vacuum appears ordered, but globally, watched through the lenses of spatial-averaging, it looks smudged into a disordered zero. It would be interesting to find out what happens with the stripe phase in the GW model. We would like to see how its renormalizability plays out from the phase transition point of view.

Phase diagrams on NC spaces have been extensively studied in various matrix models, since they regularize corresponding continuum theories in a numerical simulation-friendly fashion [26–46]. They generically feature three phases that meet at a triple point. Two are readily present in commutative theories: in the disordered phase, field eigenvalues clump around zero, and in the ordered phase around one of the mirror image-minima of the potential. The third is a matrix counterpart of the NC stripe phase: eigenvalues there gather both around positive and negative minimum at the same time.

In [44], we started a numerical comparison of the two-dimensional GW-model matrix regularization with ( $R$ -on) and without ( $R$ -off) the curvature term, focusing mainly on the latter. Here, we wish to present more details on the former and to see how it bares under the oscillator term switching off procedure that ensures the  $\phi_\star^4$ -model’s renormalizability [12]. Since the triple point controls the extension of the problematic stripe phase, we will try to pinpoint its location.

The paper is organized as follows. We first reintroduce the model and present its detailed  $N = 24$  phase diagrams. Then we track the  $R$ -off triple point as we increase the matrix size. Finally, we present the effects of the curvature coupling variation on the phase diagram, look at the coupled model as we turn the coupling off, and compare its limit with the uncoupled one.

## II. MATRIX MODEL

We here continue inspection of the matrix regularization  $S_N$  of (3) started in [44]. Let us reintroduce the model and walk through its main features.

If the NC strength in  $\mathfrak{h}^{\text{tr}}$  is set to  $\epsilon = 1$ , coordinates  $\mu x$  and  $\mu y$  can be represented by finitely-truncated matrices of the Heisenberg algebra in the energy basis of the harmonic oscillator

$$X = \frac{1}{\sqrt{2}} \begin{pmatrix} \sqrt{1} & \sqrt{1} & & \\ & \sqrt{2} & \sqrt{2} & \\ & & \ddots & \ddots \end{pmatrix}_{N \times N}, \quad Y = \frac{i}{\sqrt{2}} \begin{pmatrix} \sqrt{1} & -\sqrt{1} & & \\ & \sqrt{2} & -\sqrt{2} & \\ & & \ddots & \ddots \end{pmatrix}_{N \times N}. \quad (6)$$

Derivatives in model (3), analysed in the frame formalism, are realised as commutators  $\partial_\mu = [p_\mu, \cdot]$  with momenta  $p_\mu$

$$\frac{\epsilon p_1}{i\mu} = +\mu y, \quad \frac{\epsilon p_2}{i\mu} = -\mu x, \quad \frac{\epsilon p_3}{i\mu} = \mu z - \frac{1}{2}, \quad (7)$$

hence their matrix counterparts are

$$P_1 = -Y, \quad P_2 = X, \quad P_3 = \frac{1}{2}. \quad (8)$$

These identifications associate (3) with a matrix model

$$S_N = \text{Tr} (\Phi \mathcal{K} \Phi - c_r R \Phi^2 - c_2 \Phi^2 + c_4 \Phi^4), \quad (9)$$

in which the field  $\Phi$  is a  $N \times N$  hermitian matrix,  $\mathcal{K}$  the kinetic operator and  $R$  the diagonal curvature of  $\mathfrak{h}^{\text{tr}}$  space

$$\mathcal{K} \Phi = [P_\alpha, [P_\alpha, \Phi]], \quad R_{ii} = \frac{31}{2} - \begin{cases} 16i, & i < N, \\ 8N, & i = N. \end{cases} \quad (10)$$

All originally dimensionful quantities are expressed in units of NC mass scale  $\mu$ . We chose the minus sign of the mass term to enable positive  $c_2$  to parameterize the relevant portion of the phase diagram, while positive  $c_4$  ensures that  $S$  is bounded from below. They will be accompanied by the rescaled model parameters

$$\tilde{c}_2 = \frac{c_2}{N}, \quad \tilde{c}_4 = \frac{c_4}{N}. \quad (11)$$

We performed parallel hybrid Monte Carlo simulations to measure various thermodynamic observables, most important being

- heat capacity  $C = \text{Var } S / N^2$ ,
- magnetic susceptibility  $\chi = \text{Var } |\text{Tr } \Phi| / N$ ,
- distributions of eigenvalues and traces of  $\Phi$ ,

where expectation value  $\langle \mathcal{O} \rangle$  and variance  $\text{Var } \mathcal{O}$  of the observable  $\mathcal{O}$  are given by

$$\langle \mathcal{O} \rangle = \frac{\int d\Phi \mathcal{O} e^{-S}}{\int d\Phi e^{-S}}, \quad \text{Var } \mathcal{O} = \langle \mathcal{O}^2 \rangle - \langle \mathcal{O} \rangle^2. \quad (12)$$

Phase transitions in finite systems form smeared finite peaks and edges in profiles of free energy derivatives. Different quantities yield slightly different estimates of transition points, but they ultimately converge for large enough matrices. To locate them, we scanned through parameter space by varying  $c_2$  at fixed  $c_4$ , which played a role of temperature, and searched for peaks in  $C$  and  $\chi$ .

Classical equation of motion for  $S_N$

$$2\mathcal{K}\Phi - c_r \{R, \Phi\} + \Phi (-2c_2 + 4c_4 \Phi^2) = 0, \quad (13)$$

gives us an idea what kind of phases to expect. Its kinetic, curvature and pure potential parts are respectively solved by

$$\Phi \propto \mathbb{1}, \quad \Phi = 0, \quad \Phi^2 = \begin{cases} 0, & c_2 \leq 0, \\ \frac{c_2 \mathbb{1}}{2c_4}, & c_2 > 0, \end{cases} \quad (14)$$

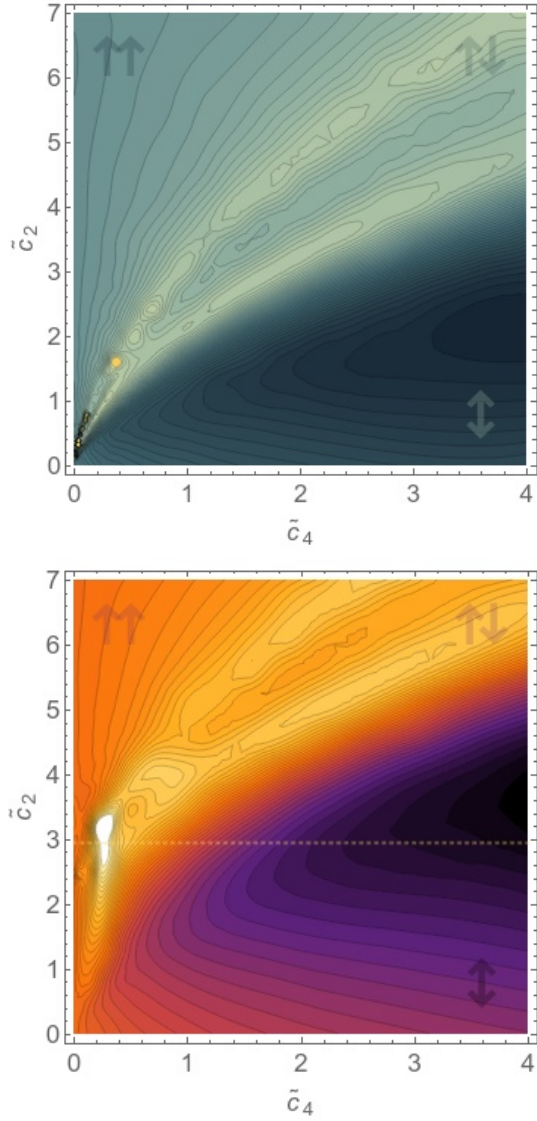


FIG. 1. Contour plots of  $N = 24$  phase diagram for  $c_r = 0$  (top) and for  $c_r = 0.2$  (bottom). Darker colors depict lower and lighter colors higher values of specific heat, bright stripes being the transition lines. The dotted line on the bottom plot indicates a diagram shift relative to the  $R$ -off case. Diagrams are constructed based on more than 4000 points.

corresponding to three phases depicted<sup>2</sup> in FIG. 1:

- disordered  $\uparrow\downarrow$ -phase:  $\langle \Phi \rangle_{\uparrow\downarrow} = 0$ ,
- uniformly ordered  $\uparrow\uparrow$ -phase:  $\langle \Phi \rangle_{\uparrow\uparrow} \propto \mathbb{1}$ ,
- non-uniformly ordered  $\uparrow\downarrow$ -phase:  $\langle \Phi \rangle_{\uparrow\downarrow} \propto U \mathbb{1}_{\pm} U^\dagger$ ,  
where  $UU^\dagger = U^\dagger U = \mathbb{1}$ ,  $\mathbb{1}_{\pm}^2 = \mathbb{1}$  and  $|\text{Tr } \mathbb{1}_{\pm}| < N$ .

<sup>2</sup> Throughout this text, we will use *Wolfram Mathematica* bluish *StarryNightColors* scheme for  $R$ -off plots and reddish *SunsetColors* scheme for  $R$ -on plots.

The  $\uparrow\downarrow$ -phase is a matrix equivalent of the stripe phase. Large mass parameter lives in  $\uparrow\uparrow$ -phase, and large quartic coupling in  $\uparrow\downarrow$ -phase, with  $\uparrow\downarrow$ -phase nested in between.

When the kinetic term is negligible (e.g. field near  $\propto \mathbb{1}$ ) and  $c_2 \geq \max_j \{c_r |R_{jj}|\}$ , a diagonal solution exists that combines the effects of the curvature and the potential and which deforms the vacuum of the ordered phases:

$$\Phi^2 = \frac{c_2 \mathbb{1} + c_r R}{2c_4}. \quad (15)$$

Both transitions out of the stripe phase in the  $R$ -off case (FIG. 1) follow the square root behaviour for larger quartic coupling. For  $\tilde{c}_4 > 1$ , they are well approximated by:

$$\uparrow\downarrow \rightarrow \uparrow\downarrow: \quad \tilde{c}_2 = 2.67(6)\sqrt{\tilde{c}_4} - 0.55(9), \quad (16a)$$

$$\uparrow\downarrow \rightarrow \uparrow\uparrow: \quad \tilde{c}_2 = 3.99(5)\sqrt{\tilde{c}_4} - 0.90(7). \quad (16b)$$

For comparison, a pure potential model would show a  $\uparrow\downarrow \rightarrow \uparrow\downarrow$  transition line  $\tilde{c}_2 = 2\sqrt{\tilde{c}_4}$  in the infinite  $N$  limit.

In [44] we presented a simple argument that, due to diagonality, curvature acts as a quasi-mass term and should shift transition lines proportionally to the  $c_r$  by  $\delta\tilde{c}_2$  relative to the  $R$ -off case:

$$\frac{1}{2N} \leq \frac{\delta\tilde{c}_2}{c_r} \leq 16 - \frac{63}{2N}. \quad (17)$$

We previously demonstrated this by numerical simulation at a token value of quartic coupling and with the absent kinetic term; here, we expose this effect in full in FIG. 1. Similar shifting is in the meantime also reported on the fuzzy sphere after adding a modification to the kinetic term [46]. The detailed analysis of the curvature's effects on the phase diagram is ongoing and will be presented elsewhere, while here we concentrate only on the aspects relevant to the position of the triple point.

We wish to simultaneously inspect two finite limits of our matrix model, which zoom-in on different portions of the phase diagram:

$$\mathcal{S} = \lim_{N \rightarrow \infty} \frac{\langle S_N(c_2, c_4, c_r) \rangle}{N^2}, \quad (18a)$$

$$\tilde{\mathcal{S}} = \lim_{N \rightarrow \infty} \frac{\langle S_N(\tilde{c}_2, \tilde{c}_4, c_r) \rangle}{N^2}, \quad (18b)$$

$\mathcal{S}_0$  and  $\tilde{\mathcal{S}}_0$  referring to  $c_r = 0$ .  $\mathcal{S}$  is closely related to  $S_{\text{GW}}$  up to a light adjustment of coefficients (Appendix A) and is focused on the neighbourhood of the origin, while  $\tilde{\mathcal{S}}_0$  is the limit we addressed in [44] which is focused on the 3rd order  $\uparrow\downarrow \rightarrow \uparrow\downarrow$  transition line.

### III. $R$ -OFF TRIPLE POINT

In [44], we found that the triple point of  $\tilde{\mathcal{S}}_0$  lies at  $\tilde{c}_4(T) \lesssim 0.005$  ( $c_4 \lesssim 0.14$  at  $N = 28$ ) and established the descending trend of  $\tilde{c}_4(T)$  with increase in matrix size. In the meantime, we collected more data for matrix sizes

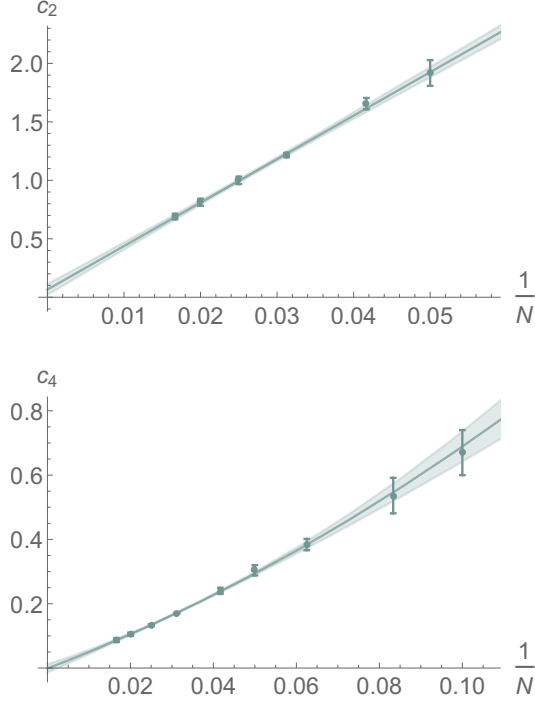


FIG. 2. Shrinking of the  $R$ -off  $\downarrow\rightarrow\uparrow\uparrow$  transition line with an increase in matrix size. **(top)** Linear fit of the endpoint's  $c_2$  as a function of the inverse matrix size  $1/N$ :  $c_2(T|r) = +0.07(5) + 37(2)/N$ . **(bottom)** Quadratic fit of the endpoint's  $c_4$  as a function of the inverse matrix size  $1/N$ :  $c_4(T|r) = -0.001(13) + 4.9(8)/N + 20(11)/N^2$ . Data gathered from susceptibility  $\chi$  for  $N \leq 60$ .

up to  $N = 60$ , allowing us to track the shrinking rate of the  $\downarrow\rightarrow\uparrow\uparrow$  transition line. Unexpectedly, this transition disappears entirely and the triple point collapses into the origin (FIG. 2).

Appendix B provides details on locating the triple point from raw data and different attempted data fits (Table I). We modeled small aberrations from the linear trend set by larger matrices by quadratic and power-law functions of  $1/N$ . All the estimates agree with triple point lying at the origin, and the best one bounds its coordinates to

$$(c_2, c_4)_T \leq (0.15, 0.005) \quad (19)$$

with 95% probability each, which is an order of magnitude improvement in precision.

In addition, linear extrapolation of the slopes of transition lines for  $N = 24, 32, 40, 50$  shows that they radiate from the triple point as

$$\downarrow\rightarrow\uparrow\downarrow: \quad c_2 = 7.1(8)c_4, \quad (20a)$$

$$\uparrow\downarrow\rightarrow\uparrow\uparrow: \quad c_2 = 17(1)c_4. \quad (20b)$$

This is also how the phase diagram of  $\tilde{\mathcal{S}}_0$  looks like zoomed-in around the origin, while away from it, its transition lines bend into  $\propto \sqrt{\tilde{c}_4}$ .

It is important to notice that even if the triple point of  $\mathcal{S}_0$  does not lie precisely at the origin, the triple point of  $\tilde{\mathcal{S}}_0$  will, due to  $\tilde{c}_i = c_i/N$ . This is in contrast with the  $\phi^4$ -model on the fuzzy sphere [41, 43].

#### IV. $R$ -ON SHIFT AND RENORMALIZATION

Coupling with curvature pushes the cusp of the stripe phase away from the origin proportionally to its strength (FIG. 3). The measured shift of the triple point in the  $N = 24$ ,  $R$ -on case

$$\tilde{c}_2(T|r) = 0.18(8) + 15.5(7)c_r \quad (21)$$

relative to the  $R$ -off value

$$\tilde{c}_2(T|r') = 0.14(5), \quad (22)$$

agrees well with the maximal prediction allowed by (17):

$$\max \delta \tilde{c}_2 = \left(16 - \frac{63}{2N}\right) c_r \approx 14.7 c_r. \quad (23)$$

The slight overshoot is discussed in Appendix B. FIG. 2 shows that intercept of  $\tilde{c}_2(T|r)$  goes to zero with the increase in matrix size, so it is safe to assume that proportionality to  $c_r$  becomes exact in the infinite size limit.

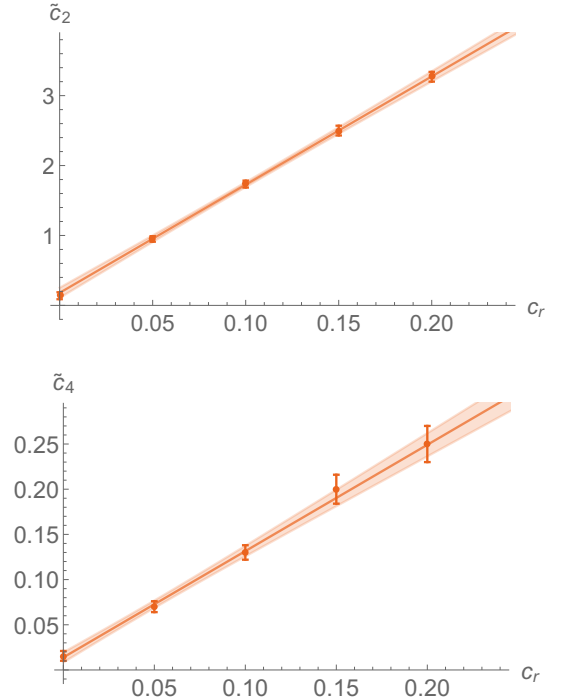


FIG. 3. Shift of the cusp of the stripe phase, with rising curvature coupling:  $\tilde{c}_2(T|r) = 0.18(8) + 15.5(7)c_r$ ,  $\tilde{c}_4(T|r) = 0.014(6) + 1.19(8)c_r$ . Data gathered from specific heat  $C$  for  $N = 24$ .



In the GW approach [12], renormalizability of the limiting  $\phi_\star^4$ -model is assured by taking

$$\frac{1 - \Omega^2}{1 + \Omega^2} = \sqrt{1 - \frac{1}{(1 + \log(\Lambda_0/\Lambda_R))^2}}, \quad (24)$$

which for large cutoff  $\Lambda_0 \propto \sqrt{N}$  switches  $\Omega$  off as

$$\Omega \sim \frac{1}{\log N}. \quad (25)$$

Since we in Appendix A identify  $\Omega$  and  $c_r$  as

$$c_r = \frac{\Omega^2/8}{1 - \Omega^2/2}, \quad (26)$$

we consider the limit where  $c_r$  decreases as

$$c_r \sim \frac{1}{\log^2 N}. \quad (27)$$

Combining this with  $\delta\tilde{c}_2 \propto c_r$ , or rather  $\delta c_2 \propto c_r N$ , would effectively swipe the stripe phase off to infinity as

$$\frac{N}{\log^2 N}, \quad (28)$$

leaving the renormalized model with a completely different phase diagram from the one obtained by simply setting  $c_r = 0$ .

Looking back at the equation of motion (13) and its solutions (14), we see that curvature term prefers the trivial over striped vacuum. The action (9) also shows that the curvature itself compensates the attenuation of the coupling. For nearly ordered field configurations  $\Phi^2 \propto \mathbb{1}$ , the curvature term dominates the potential by factor

$$\frac{\text{Tr } R \Phi^2}{\text{Tr } \Phi^{2n}} \approx \frac{\text{Tr } R}{\text{Tr } \mathbb{1}} = -8N \left(1 - \frac{31}{16N}\right) \sim N, \quad (29)$$

which multiplied by the coupling leads once more to

$$\frac{N}{\log^2 N}. \quad (30)$$

This somewhat unusual situation is perhaps best understood with the help of *The Little Prince*. If we, by chance, stumble in the dark upon a snake from the narrator's drawing, judging by its thin tail, we would conclude that it is pretty hungry. But once the light is on, we would see that it has, in fact, swallowed an elephant.

## V. CONCLUDING REMARKS

This paper aimed to see if the GW-model's renormalizability is reflected in its corresponding phase diagram and if it affects the extent of the stripe phase connected to the UV/IR mixing. With that in mind, we tracked the positions of the triple point of the matrix regularization of the model: this is where the stripe phase starts,

spreading towards larger values of the mass and quartic parameters. We compared the model with and without the curvature term since its inclusion is crucial to the model's renormalizability.

We first refined the estimate [44] of the triple point position in the case of no coupling with the curvature. We conclude that it collapses to the origin in the infinite matrix size limit, completely erasing the  $\downarrow \rightarrow \uparrow \uparrow$  transition line.

When the curvature coupling activates, it shifts the triple point and the transition lines towards larger values of the mass parameter, proportionally to its strength and the matrix size. GW coupling attenuation procedure does not reverse this effect. Instead, the triple point seems to be expelled to infinity, taking the stripe phase away with it.

This leads to different phase diagrams for renormalized and non-renormalized  $\phi_\star^4$ -model. The former seems to be stripe phase-free, while in the latter, the stripe phase is tethered to the origin of the parameter space.

We are currently completing the exploration of the  $R$ -on model, and we plan to further inspect the  $R$ -off triple point for  $N > 60$  to make sure it lies at the origin. Although we observed the convincing curvature-mediated linear shift for  $N = 24$ , it would be prudent to confirm the effect for larger matrices as well. We would also like to simultaneously decrease the coupling and increase the matrix size since their combined effect was indirectly deduced.

Additionally, we mean to revisit the GW-inspired gauge model [22] in the hope of uncovering the reverse effect: non-renormalizability due to retention of the stripe phase. After fixing the NC strength and scale, the model is left with only one adjustable parameter — the field strength coupling  $g$ . Its additional stripe-like vacuum (5) transforms into a trivial one for the infinite coupling, implying the phase diagram's possible structure: stripe phase for small  $g$ , disordered phase for large  $g$ .

Another possible line of investigation could be the phase diagram of renormalizable spinor model on  $\mathfrak{h}^{\text{tr}}$  [47] in context of fermionic matrix models [48, 49].

If this correspondence between renormalizability and phase structure proves to hold across models, it might be helpful when constructing new ones. It could be possible to search numerically for early signatures of (non)renormalizability in their phase diagrams, assessing the new model's renormalizability potential, even before the involved and time-consuming analytical exploration.

## ACKNOWLEDGMENTS

This work was supported by the Serbian Ministry of Education, Science and Technological Development Grant ON171031 and by COST Action MP1405. The author would like to thank Prof Maja Burić, Prof Denjoe O'Connor, and Dr. Samuel Kováčik for valuable discussions and DIAS for hospitality and financial support.

## Appendix A: Model correspondence

According to [39], mapping

$$\phi \longleftrightarrow \Phi, \quad \int \longleftrightarrow \sqrt{\det 2\pi\theta} \text{Tr} \quad (\text{A1})$$

connects field theory on Moyal space and matrix field theory with the same parameters. Also, [15] provides a correspondence between  $S_{\text{GW}}$  and  $S_R$ :

$$S_{\text{GW}} = \left(1 - \frac{\Omega^2}{2}\right) S_R, \quad (\text{A2a})$$

$$m^2 = \left(1 - \frac{\Omega^2}{2}\right) \left(M^2 - \frac{15}{2}\xi\mu^2\right), \quad (\text{A2b})$$

$$\lambda = \left(1 - \frac{\Omega^2}{2}\right) \Lambda, \quad (\text{A2c})$$

$$\Omega^2 = 8\epsilon^2 \left(1 - \frac{\Omega^2}{2}\right) \xi. \quad (\text{A2d})$$

From these, by comparing (3) and (9), it is easy to conclude that  $S_{\text{GW}}$  and  $S_N$  are connected by

$$S_{\text{GW}} = \pi \left(1 - \frac{\Omega^2}{2}\right) S_N, \quad (\text{A3a})$$

$$m^2 = - \left(1 - \frac{\Omega^2}{2}\right) \left(c_2 + \frac{15}{2}c_r\right), \quad (\text{A3b})$$

$$\lambda = 12 \left(1 - \frac{\Omega^2}{2}\right) c_4, \quad (\text{A3c})$$

$$\Omega^2 = 8 \left(1 - \frac{\Omega^2}{2}\right) c_r, \quad (\text{A3d})$$

in the large  $N$  limit ( $\theta^{12} = 1/\mu^2$ , units:  $\mu = 1$ ). Furthermore, action multiplier can be absorbed into the field during expectation value integration and will affect only  $c_4$ :

$$\langle \kappa S(c_2, c_4, c_r) \rangle_{\kappa S} = \langle S(c_2, c_4/\kappa, c_r) \rangle_S, \quad (\text{A4a})$$

$$\sqrt{\kappa} \langle \Phi \rangle_{\kappa S}(c_2, c_4, c_r) = \langle \Phi \rangle_S(c_2, c_4/\kappa, c_r), \quad (\text{A4b})$$

yielding

$$C_{\kappa S}(c_2, c_4, c_r) = C_S(c_2, c_4/\kappa, c_r), \quad (\text{A5a})$$

$$\kappa \chi_{\kappa S}(c_2, c_4, c_r) = \chi_S(c_2, c_4/\kappa, c_r). \quad (\text{A5b})$$

Since we are interested in the position of peaks of  $C$  and  $\chi$ , this means that phase transition diagrams for  $\kappa S$  and  $S$  will be the same up to a reparametrization

$$(c_2, c_4, c_r) \longleftrightarrow (c_2, c_4/\kappa, c_r). \quad (\text{A6})$$

For phase diagrams of  $S_{\text{GW}}$  and  $S$  in the  $\Omega \rightarrow 0$  limit ( $c_r \rightarrow 0$ ), this means:

$$(m^2, \lambda) \longleftrightarrow (-c_2, 12c_4/\pi). \quad (\text{A7})$$

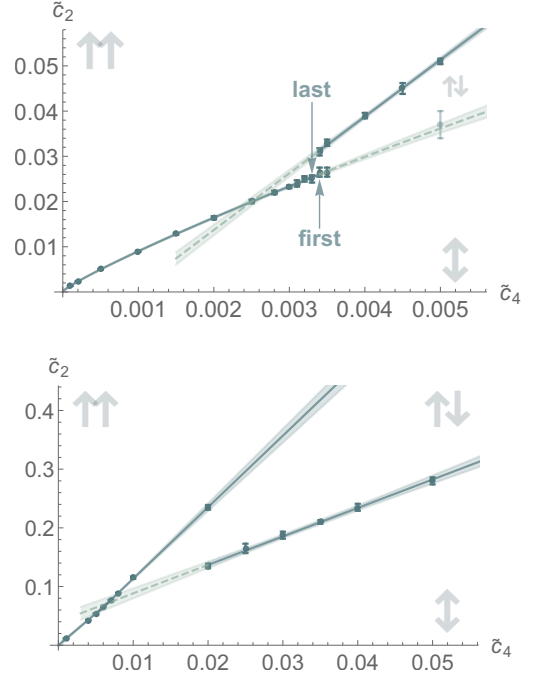


FIG. 4. (top) Change in slope of the edge of  $\uparrow\uparrow$ -phase indicates a triple point. Arrows mark the last point on  $\uparrow\downarrow \rightarrow \uparrow\uparrow$  and the first point on  $\uparrow\downarrow \rightarrow \uparrow\downarrow$  lines. Constructed from  $\chi$ -data for  $N = 40$ . (bottom) Extrapolated transition lines with 83% confidence intervals. Constructed from  $C$ -data for  $N = 40$ .

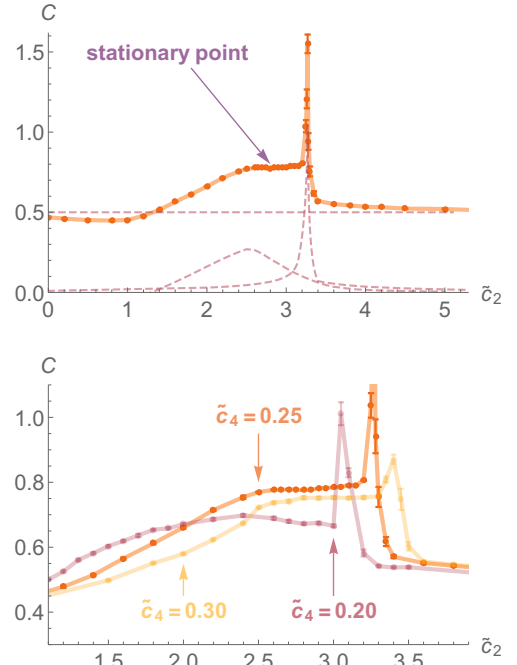


FIG. 5. (top) Triple point region for  $N = 24$ ,  $c_r = 0.2$  at  $\tilde{c}_4 = 0.25$  resolved into two peaks. The stationary point at the plateau is chosen as the triple point proxy. (bottom) Plateau at  $\tilde{c}_4 = 0.25$  mounts above plateaus at  $\tilde{c}_4 = 0.20$  and  $\tilde{c}_4 = 0.30$ , building a wall between phases.

TABLE I. Different models of  $R$ -off triple point position fitting. All intercepts are consistent with the triple point located at the origin. A linear fit is performed for data subsets with higher  $N$ , where nonlinearities are imperceptible.

data	model	$c_4$ -fit	$c_2$ -fit
$\chi$	linear	$c_4 = -0.012(11) + 5.9(4)/N$	$c_2 = +0.07(5) + 37(2)/N$
	quadratic	$c_4 = -0.001(13) + 4.9(8)/N + 20(11)/N^2$	$c_2 = +0.04(8) + 39(5)/N - 42(60)/N^2$
	power law	$c_4 = +0.016(17) + 12(4)/N^{1.25(13)}$	$c_2 = -0.0(2) + 31(10)/N^{0.93(14)}$
$C$	linear	$c_4 = -0.12(10) + 16(3)/N$	$c_2 = +0.9(9) + 93(21)/N$

## Appendix B: Triple point proxies and fits

We here discuss triple point proxies used for FIG. 2 and FIG. 3.

In FIG. 4, the split of the profile of  $\chi$  into two separate peaks changes the slope of the  $\uparrow\uparrow$ -phase border  $\partial_{\uparrow\uparrow}$ . The midpoint between the last point in one-peak and the first point in the two-peak regime served as the triple point proxy for FIG. 2. We used the standard deviation of the triangular distribution ending at these two points as the triple point position uncertainty. For  $N \leq 24$ , the two peaks are not completely separated in the triple point region, so we took the intersection of extrapolated transition lines instead.

For consistency, we also checked the  $C$ -data, which has less predictive power due to larger uncertainties and distance from the triple point region. We extrapolated  $\uparrow\rightarrow\uparrow\downarrow$  transition line to its intersection with  $\partial_{\uparrow\uparrow}$ . To get 68% confidence intervals of the intersection point coordinates, we used 83% confidence intervals of transition line fits, since the probability of triple point belonging to their intersection is given by

$$P(\uparrow\rightarrow\uparrow\downarrow \cap \partial_{\uparrow\uparrow}) = P(\uparrow\rightarrow\uparrow\downarrow)P(\partial_{\uparrow\uparrow}) \quad (\text{B1})$$

and  $0.68 \approx 0.83^2$ .

In the  $R$ -on case, we used contour diagrams (e.g. FIG. 1) to detect the cusp of the  $\uparrow\downarrow$ -phase from  $C$ -data. We looked at the bright triple point peak position and then checked the neighboring raw data to pinpoint its exact location. As it turns out, the peak resolves into two very closely spaced convoluted peaks – which presumably coincide when matrix size increases – joined by a wall that separates phases (FIG. 5). For FIG. 3, we used the position of the protruding peak, which gave a slightly higher estimate for the slope than (23). The stationary point on this wall seems a more realistic estimator of the triple point position, but it is also more difficult to measure. A rough estimate using the stationary point

$$\tilde{c}_2(T|r) = 13.2(11)c_r + 0.24(9), \quad (\text{B2})$$

fits within the interval (17) and is close to its upper bound. For comparison, the slope of the line connecting the smaller peaks is around 12.

Looking at FIG. 1, we see a small elliptical local minimum-region with a bright triple point peak at its lower left edge. Eigenvalue distribution there has the characteristics of the  $\uparrow\downarrow$ -phase. We do not believe this to constitute a separate phase but a finite-size effect that collapses into a triple point as the matrix size increases. This should be, of course, checked at larger  $N$ .

The different extrapolations of the triple point position in the infinite matrix limit are collected in TABLE I.

- 
- |  |   |
|--|---|
| <p>[1] L. Carroll, <i>Alice's Adventures in Wonderland</i> (The Project Gutenberg EBook, 2008).</p> <p>[2] M. Bayley, <i>New Scientist</i> <b>204</b>, 38 (2009).</p> <p>[3] H. S. Snyder, <i>Phys. Rev.</i> <b>71</b>, 38 (1947).</p> <p>[4] J. Bellissard, A. van Elst, and H. Schulz-Baldes, <i>Journal of Mathematical Physics</i> <b>35</b>, 5373 (1994), <a href="https://doi.org/10.1063/1.530758">https://doi.org/10.1063/1.530758</a>.</p> <p>[5] K. Fujii, (2005), <i>quant-ph/0502174</i>.</p> <p>[6] N. Seiberg and E. Witten, <i>JHEP</i> <b>09</b>, 032 (1999), <i>hep-th/9908142</i>.</p> <p>[7] S. Minwalla, M. Van Raamsdonk, and N. Seiberg, <i>JHEP</i> <b>02</b>, 020 (2000), <i>hep-th/9912072</i>.</p> <p>[8] C.-S. Chu, J. Madore, and H. Steinacker, <i>JHEP</i> <b>08</b>, 038 (2001), <i>hep-th/0106205</i>.</p> | <p>[9] B. P. Dolan, D. O'Connor, and P. Presnajder, <i>JHEP</i> <b>03</b>, 013 (2002), <i>hep-th/0109084</i>.</p> <p>[10] C. P. Martin, J. Trampetić, and J. You, <i>UV/IR mixing in Noncommutative SU(N) Yang-Mills theory</i>, 2020.2012.09119.</p> <p>[11] E. Langmann and R. J. Szabo, <i>Physics Letters B</i> <b>533</b>, 168–177 (2002).</p> <p>[12] H. Grosse and R. Wulkenhaar, <i>JHEP</i> <b>12</b>, 019 (2003), <i>hep-th/0307017</i>.</p> <p>[13] M. Disertori, R. Gurau, J. Magnen, and V. Rivasseau, <i>Phys. Lett. B</i> <b>649</b>, 95 (2007), <i>hep-th/0612251</i>.</p> <p>[14] Z. Wang, <i>Annales Henri Poincaré</i> <b>19</b>, 2435 (2018), 1805.06365.</p> <p>[15] M. Buric and M. Wohlgenannt, <i>JHEP</i> <b>03</b>, 053 (2010),</p> |
|--|---|

- 0902.3408.
- [16] S. A. Franchino-Viñas and S. Mignemi, Eur. Phys. J. C **80**, 382 (2020), 1911.08921.
  - [17] M. Buric, D. Latas, and L. Nenadovic, Eur. Phys. J. C **78**, 953 (2018), 1709.05158.
  - [18] M. Buric and D. Latas, Phys. Rev. D **100**, 024053 (2019), 1903.08378.
  - [19] D. N. Blaschke, Fortsch. Phys. **62**, 820 (2014), 1402.5980.
  - [20] M. Buric, H. Grosse, and J. Madore, JHEP **07**, 010 (2010), 1003.2284.
  - [21] M. Buric, M. Dimitrijevic, V. Radovanovic, and M. Wohlgenannt, Phys. Rev. D **86**, 105024 (2012), 1203.3016.
  - [22] M. Burić, L. Nenadović, and D. Prekrat, Eur. Phys. J. C **76**, 672 (2016), 1610.01429.
  - [23] S. S. Gubser and S. L. Sondhi, Nucl. Phys. B **605**, 395 (2001), hep-th/0006119.
  - [24] P. Castorina and D. Zappala, Phys. Rev. D **77**, 027703 (2008), 0711.2659.
  - [25] H. Mejía-Díaz, W. Bietenholz, and M. Panero, JHEP **10**, 056 (2014), 1403.3318.
  - [26] D. J. Gross and E. Witten, Phys. Rev. D **21**, 446 (1980).
  - [27] X. Martin, JHEP **04**, 077 (2004), hep-th/0402230.
  - [28] M. Panero, JHEP **05**, 082 (2007), hep-th/0608202.
  - [29] D. O'Connor and C. Saemann, JHEP **08**, 066 (2007), 0706.2493.
  - [30] F. Garcia Flores, X. Martin, and D. O'Connor, Int. J. Mod. Phys. A **24**, 3917 (2009), 0903.1986.
  - [31] F. Lizzi and B. Spisso, Int. J. Mod. Phys. A **27**, 1250137 (2012), 1207.4998.
  - [32] A. P. Polychronakos, Phys. Rev. D **88**, 065010 (2013), 1306.6645.
  - [33] J. Tekel, JHEP **10**, 144 (2014), 1407.4061.
  - [34] B. Ydri, JHEP **03**, 065 (2014), 1401.1529.
  - [35] S. Rea and C. Sämann, JHEP **11**, 115 (2015), 1507.05978.
  - [36] J. Tekel, Acta Phys. Slov. **65**, 369 (2015), 1512.00689.
  - [37] J. Tekel, JHEP **12**, 176 (2015), 1510.07496.
  - [38] B. Ydri, K. Ramda, and A. Rouag, Phys. Rev. D **93**, 065056 (2016), 1509.03726.
  - [39] B. Ydri *Lectures on Matrix Field Theory* Vol. 929 (Springer, 2017), 1603.00924.
  - [40] P. Sabella-Garnier, JHEP **08**, 121 (2017), 1705.01969.
  - [41] J. Tekel, Phys. Rev. D **97**, 125018 (2018), 1711.02008.
  - [42] K. Hatakeyama, A. Tsuchiya, and K. Yamashiro, PTEP **2018**, 063B05 (2018), 1805.03975.
  - [43] S. Kováčik and D. O'Connor, JHEP **10**, 010 (2018), 1805.08111.
  - [44] D. Prekrat, K. N. Todorović-Vasović, and D. Ranković, JHEP **03**, 197 (2021), 2002.05704.
  - [45] M. Šubjaková and J. Tekel, PoS **CORFU2019**, 189 (2020), 2006.12605.
  - [46] M. Šubjaková and J. Tekel, JHEP **06**, 088 (2020), 2002.02317.
  - [47] M. Burić, J. Madore, and L. Nenadovic, Class. Quant. Grav. **32**, 185018 (2015), 1502.00761.
  - [48] G. W. Semenoff and R. J. Szabo, Int. J. Mod. Phys. A **12**, 2135 (1997), hep-th/9605140.
  - [49] I. Aref'eva and I. Volovich, JHEP **10**, 114 (2019), 1902.09970.